Desalination and Water Treatment
www.deswater.com
doi: 10.5004/dwt.2021.27392

229 (2021) 331–342
July

Modification of graphitic carbon nitride photocatalyst by Pb-contaminated water for efficient removal of cefixime from aqueous media

Foroogh Salehi[a], Samad Sabbaghi[a,b,*], Naghmeh Sadat Mirbagheri[b]

[a]*Nanochemical Engineering Department, Faculty of Advanced Technologies, Shiraz University, Shiraz, Iran, emails: sabbaghi@shirazu.ac.ir (S. Sabbaghi), ssforoogh@gmail.com (F. Salehi)*
[b]*Drilling Nano Fluid Lab. Shiraz University, Shiraz, Iran, email: n.s.mirbagheri@gmail.com*

Received 17 July 2020; Accepted 5 May 2021

ABSTRACT

In this study, graphitic carbon nitride (g-C_3N_4) and its modified form with Pb wastewater were prepared with a thermal polymerization method at 520°C for 2 h with a 10°C/min heating rate. The prepared composites were used as active catalysts in visible light to remove cefixime from aqueous solutions. Various factors such as the initial concentration of the contaminant, catalyst loading, process time, and initial pH on cefixime removal were efficiently studied in this research. The results indicate that the modified catalyst has a better performance in cefixime removal than g-C_3N_4. Design-Expert software was performed to design experiments and find optimum conditions to achieve maximum cefixime removal efficiency by Pb doped g-C_3N_4. The maximum removal percentage was observed is 84%, which achieved at optimum conditions obtained by the design of experiments software (cefixime's initial concentration of 47 mg/L, 1.7 g/L catalyst loading, 113 min process time, and initial pH of 6.2). Moreover, the removal process was done in continuous cycles at the optimum conditions to investigate the economic aspect and the results showed removal efficiency decreases from 84% to 37% in five cycles. One of the most notable novelties of this work is using lead as a water pollutant material, to make a new photocatalyst for cefixime removal.

Keywords: Cefixime; Lead; Graphitic carbon nitride; Photocatalyst; Wastewater treatment

1. Introduction

The lack of healthy water sources due to population growth, industry development, and increasing demands is a universal concern [1]. The mentioned reasons increase the use of medicine, which predicted a 24% increment in using pharmaceuticals from 2015 until 2020 [2]. Pharmaceuticals have an important role in the human and animal healthcare, which have been used for a long time. Observing some medicines such as painkillers for the first time in the USA's water in the seventies, propose pharmaceuticals as an environment pollutant [3,4]. Although the amount of these pharmaceuticals in the environment is low, their presence in water is still a threat for the livings, since they are designed to be highly effective in low concentrations. Antibiotics are a type of pharmaceutical materials designed to treat bacterial infections. According to the World Health Organization (WHO), antibiotic resistance is one of the biggest threats to global health in 20th century. Besides, cefixime is a widely used antibiotic which its existence in water is evident [5–8].

Conventional methods for wastewater treatment that use for removing suspended particles and organic compounds cannot be employed for pharmaceutical products due to their complex chemical structures [9]. In reality, refineries are known as pollutant sources themselves for these kinds of pollution, and its critical to use a suitable method for pharmaceutical pollution removal [10].

* Corresponding author.

Nowadays, the use of antibiotics in the medical field increases, and also the probability of their presence in water increases too. Hence, it is important to find an efficient way to prevent antibiotic entrance into water sources [11–21].

In 2009, g-C_3N_4 was introduced as a new photocatalyst that the researcher focused on due to its high physical and chemical stability, reachability, ease of synthesis, and activity in the invisible zone [22].

Leong et al. [23], study the effect of a new ternary photocatalyst on amoxicillin removal by reconstructing TiO_2 with g-C_3N_4 and Ag. Their results showed the obtained ternary composite plays a significant role as an effective high visible light responsive photocatalysts for efficient removal of amoxicillin.

In 2017, Uresti et al. [24] investigated the ciprofloxacin reduction in aqueous solution by synthesizing the $PbMoO_4$/g-C_3N_4 hybrid nanocomposites loadings 0, 20, 50, 80, and 100 wt.% of $PbMoO_4$ by sonochemical method. The synthesized nanocomposites were characterized by UV-Vis diffuse reflectance spectroscopy (DRS), X-ray diffraction (XRD), scanning electron microscopy (SEM), photoluminescence (PL), and the Brunauer–Emmett–Teller (BET) method. The photoactivity of the $PbMoO_4$/g-C_3N_4 (50/50 wt.%) hybrid composite increased 11 times more than of the pure g-C_3N_4 due to its remarkable specific surface area and crystalline structure of $PbMoO_4$/g-C_3N_4 nanoparticles.

A modified Nb_2O_5/g-C_3N_4 photocatalyst was employed by Hong et al. [25] via a simple one-step heating strategy for the first time to decrease such antibiotics from water. They observed the novel photocatalyst showed significant enhancement in photocatalytic activity for the reduction of tetracycline hydrochloride both under visible and simulated solar light irradiation in comparison with pure ones; and also, the 3 wt.% Nb_2O_5/g-C_3N_4 heterojunction exhibited noticeable improvement of photocatalytic activity for the reduction of ciprofloxacin and levofloxacin. This increment in photoactivity can be due to the formation of a heterojunction between g-C_3N_4 and Nb_2O_5, which can suppress the photogenerated electron–hole pair's recombination.

In similar research, Wang et al. [26] studied the tetracycline removal from aqueous solutions by synthesizing TiO_2/g-C_3N_4 core-shell quantum heterojunction. They reported photoactivity through Tetracycline removal was improved. Moreover, 100 mg of TiO_2/g-C_3N_4 photocatalyst demonstrated the highest tetracycline reduction rate of 2.2 mg/min, which is 2.3 times higher than pure g-C_3N_4, 36% higher compared to TiO_2/g-C_3N_4 random mixture, and 2 times higher than pure TiO_2. They also proposed h^+ and O_2^- as the main oxidants for the efficient photocatalytic reaction.

Li et al. [27] focused on Tetracycline hydrochloride degradation from water using the novel Z-scheme mes-Sn_3O_4/g-C_3N_4 heterostructure and observed higher degradation than pure g-C_3N_4. These consequences can be because of a larger specific surface area which is affected by the presence of Sn_3O_4 on g-C_3N_4 nanosheets.

Sheydaei et al. synthesized nano n-TiO_2/graphene oxide/titan grid sheets by immobilizing graphene oxide and nitrogen doped TiO_2 on titan grid sheets by an electrophoretic deposition method. They characterized prepared nanocomposite by SEM, Fourier-transform infrared spectroscopy (FT-IR), DRS, and N_2 adsorption–desorption analyses and used this to investigate of the cefixime removal from water through visible light photocatalytic ozonation process. They observed cefixime degradation increased by increasing light intensity, the dosage of catalyst and ozone concentration, contact time, pH, also, by decreasing inorganic and organic scavenger and initial concentration of cefixime. Moreover, the novel catalyst showed higher performance compared to the pure one [28].

In 2017, Zavareh and Eghbalazar [29] studied on efficient and selective removal of cefixime from aqueous solution by a modified Cu–chitosan/Al_2O_3 nanocomposite by adsorption isotherms and kinetic studies at room temperature. Their results indicated much higher removal efficiency and selectivity for modified nanocomposite compared to neat chitosan. Moreover, the nanocomposite showed good recyclability through several adsorption-desorption cycles.

Cefixime removal from aqueous solution was investigated by Rasoulifard et al. [30]. They used a modified hardened paste of Portland cement by perlite with various factors such as adsorbent dosage, adsorbate concentration, contact time, type of adsorbent, and pH in their study.

In this research, Pb-doped g-C_3N_4 was used to remove cefixime from wastewater. g-C_3N_4 is a cost-effective polymeric photocatalyst with a facile synthesis procedure which makes this catalyst more valuable. To synthesis modified photocatalyst, Pb wastewater was used with g-C_3N_4, that is one of the remarkable innovations of this study which wastewater (Pb contaminated water) used to reduce an antibiotic (cefixime) from wastewater.

In this study, two aims were pursued simultaneously. First, removing cefixime from aqueous solution by a photocatalytic process. Second, using of a Pb-containing wastewater for removing cefixime.

2. Experimental procedure

2.1. Materials

Melamine (2,4,6-Triamino-1,3,5-triazine, Merck, 99%), hydrochloric acid (HCl, 37%), sodium hydroxide (NaOH, 97%) were purchased from Merck Co. Lead(II) nitrate ($Pb(NO_3)_2$, 99%), cefixime 100 oral suspension powder, and double distilled water (DDW) were purchased from Acros, Loghman Pharmaceutical & Hygienic, and Zolal, companies respectively. All of the chemical reagents used in this paper were of analytical grade and were used without further purification.

2.2. Synthesis of the photocatalysts

The photocatalyst synthesis was consist of two steps, the first step involved melamine annealing for pure g-C_3N_4 preparation (based on a thermal polymerization), and the second step involved the synthesis of Pb-doped g-C_3N_4 composites by Pb contaminated water with expected concentration [31]. Initially, 1 g of melamine was calcined in the furnace at 520°C for 2 h with a ramping speed of 10°C/min to prepare pure g-C_3N_4. Eventually, after calcination, yellow g-C_3N_4 was synthesized [32]. In the following,

to synthesize Pb-doped g-C_3N_4, 1 g of melamine was added to 2 ml of Pb-contaminated water at specified concentrations (800; 1,600; 2,400 and 3,200 mg/L), and obtain solution was stirred for 2 h. The obtaining suspension was dried in an oven at 100°C for 12 h, and then the product was grounded to a fine powder. The powder was calcined for 2 h at 520°C with a ramping speed of 10°C/min. After cooling to room temperature, the obtained products were collected and milled into powder in an agate mortar for further use. To make clarity, the Pb-doped g-C_3N_4 composites with various concentration of 800; 1,600; 2,400 and 3,200 mg/L, were mentioned as Pb/CN-1, Pb/CN-2, Pb/CN-3, Pb/CN-4, respectively, in the manuscript.

2.3. Characterization

The powder X-ray diffraction patterns were recorded by using the PANalytical X'Pert Pro-MPD Powder Diffractometer operating with Cu-Ka source to investigate the crystal structure of the samples. The measurement was performed at 40 kV and 30 mA (l¼ 1.5418 Å). The morphologies of resulting samples were characterized by a field emission-scanning electron microscopy (FE-SEM, MIRA3 TESCAN-XMU) at 30 kV. The functional group spectrums were analyzed using Fourier-transform infrared spectrometer recorded in 400–4,000 cm^{-1} range (FT-IR, Bruker, TENSOR II, USA). Moreover, the specific surface area of samples was characterized by the nitrogen absorption–desorption data and BET measurement at 77 K (ASAP2020, Micromeritics, USA). Before the analysis, the sample was outgassed for 3 h at 150°C under vacuum conditions.

2.4. Cefixime solution preparation

A cefixime 100 oral suspension powder was grounded in an agate mortar. A 100 mg/L cefixime solution was prepared by dissolving 150 mg of the powder in 100 mL water and stirring for 60 min. Afterward, the solution was filtered and kept in a non-transparent container and was used for preparing various concentrations of solution (10, 25, 40, 55, and 70 mg/L) daily by diluting.

2.5. Photocatalytic experiments

The photocatalytic activities were evaluated through decomposing cefixime under visible light irradiation by using a 500 W linear tungsten–halogen lamp with high-pass UV filter (FSQ-GG400, Newport Corp). In a typical procedure, a homogeneous suspension was prepared by dispersing a certain amount of photocatalyst in the aqueous solution of cefixime. Before irradiation, the mixture was magnetically stirred for 70 min in the dark to establish an adsorption-desorption equilibrium. After a certain irradiation time, the suspension was centrifuged to remove the photocatalyst particles, and the collected solution was analyzed by a UV-Vis spectrophotometer (V-730, JASCO Corporation, Japan) at λ_{max} = 288.5 nm. While the cefixime removal percentage was expressed as the following:

$$\text{Removal}(\%) = \frac{C_0 - C_t}{C_t} \times 100 \quad (1)$$

where C_0 and C_t are the concentrations (mg/L) of cefixime at t = 0 and at a given time interval, respectively.

3. Results and discussion

In this section, modified g-C_3N_4 nanosheets with Pb wastewater characterization, the effect of nanosheets modification and Pb concentration on the composite's performance, and cefixime efficient removal will be discussed.

3.1. Characterization of synthesized photocatalyst

To characterize the prepared g-C_3N_4 and modified g-C_3N_4, XRD, FT-IR, FE-SEM, energy-dispersive X-ray spectroscopy (EDX), and BET analyses were obtained. The results are shown as follows:

3.1.1. XRD analysis

The XRD analysis of both g-C_3N_4 and modified g-C_3N_4 was carried to investigate their crystalline structure (Fig. 1). Regarding the XRD patterns, two distinct peaks at about 13° and 27.66° were observed for both samples, which related to (100) and (002) diffraction planes of the g-C_3N_4, respectively [33,34]. It must be noted that the results are close to the results of the other reported researches [35,36].

After the Pb coordination to the g-C_3N_4, the diffraction peaks were shifted to the higher angle (from 27.66° to 27.8°), implying the interaction between the Pb and the g-C_3N_4 nanosheets [37]. The XRD pattern of Pb-doped g-C_3N_4 nanosheets shows the existence of Pb in the composite. Consequently, the intensity of the diffraction peaks of g-C_3N_4 was decreased. It demonstrated the existence of host-guest interactions between Pb and g-C_3N_4, as reported [38]. Also, the intensity of the (002) peak reduced in the presence of Pb, indicating excessive Pb was not effective in the exfoliation of g-C_3N_4 [39]. However, the main peak at 27.8° was observed in the Pb-doped g-C_3N_4 nanosheets, indicated that Pb was chemically coordinated to the g-C_3N_4 host as reported [40]. But, the (100) peak disappeared after

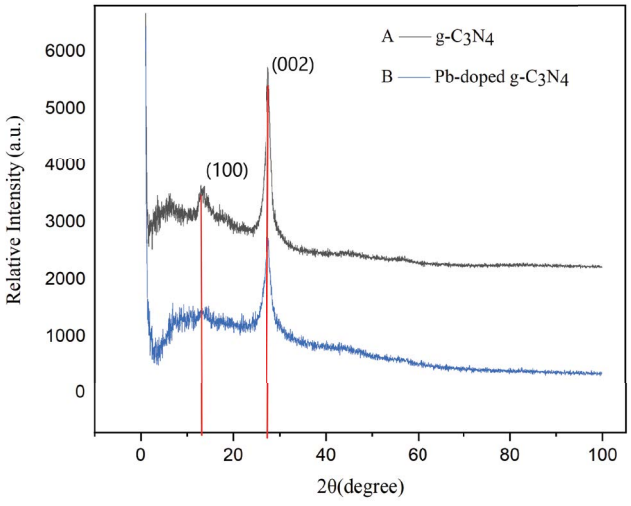

Fig. 1. XRD spectra of Pb-doped g-C_3N_4 and g-C_3N_4.

the doping of Pb, which showed that the Pb was embedded into in-planes [41], which was quite similar to other metal-doping g-C_3N_4 materials [40–43].

3.1.2. FT-IR analysis

FT-IR spectra of the same amounts of both g-C_3N_4 and modified g-C_3N_4 are shown in Fig. 2. The broad absorption band at 3,152 cm^{-1} can be originated from the N–H and O–H stretching vibrations of the adsorbed water molecules. While the absorption peak at 890 cm^{-1} may be attributed to deformation of the mode of N–H, the peaks at 804.44 cm^{-1} are related to tirs-tirazine/heptazine structures. The peaks over 1,231.2–1,628.17 cm^{-1} indicated the tensile vibrations of CN heterocycles [31,44–46]. The intensity of the multiple peaks is generally decreased after Pb-treatment due to the connection between Pb and CN aromatic rings by a coordination bond [39]. It must be noted that the FT-IR spectra of the samples are nearly the same, and no obvious difference can be seen between them, indicating that the carbon nitride chemical structure not changed during the Pb-treatment.

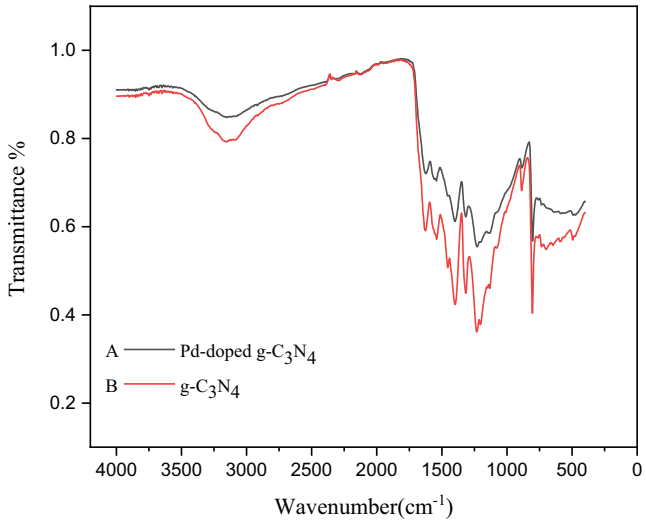

Fig. 2. FT-IR absorption spectrum of g-C_3N_4 and Pb-doped g-C_3N_4 nanosheets.

3.1.3. SEM images

The morphology and microstructure of both g-C_3N_4 (Fig. 3a) and modified g-C_3N_4 (Fig. 3b) were checked by FE-SEM. As shown in this figure, both g-C_3N_4 and modified g-C_3N_4 exhibited two-dimensional layered structures (sheets) with wrinkles. The brighter spots in Fig. 3b indicate the presence of Pb that formed like this due to the aggregation of Pb on the sheets.

3.1.4. EDX and EDX mapping analysis

The purely composed of Pb-doped g-C_3N_4 and g-C_3N_4 nanosheets were further studied by EDX analysis (Fig. 4). The Pb-doped g-C_3N_4 were consisted of C, N, and Pb elements, indicated that Pb/g-C_3N_4 had been only composed of Pb and g-C_3N_4. This increment would cause the enhancement of photocatalytic activity. The N/C molar ratio in Pb-doped g-C_3N_4 is 1.61, which is lower than the value of g-C_3N_4 (1.85). The difference in N/C value could be related to the inhibition of polymeric condensation by Pb (10.36 wt.%) [41]. Moreover, The EDX elemental mapping was performed for Pb-doped g-C_3N_4 and is presented in Fig. 5.

3.1.5. UV-Vis analysis

Fig. 6a shows the UV-Vis absorption spectra of the g-C_3N_4 and Pb-doped g-C_3N_4. The results were analyzed by a Tauc plot of the Kubelka–Munk function to estimate the bandgap energies of the same amounts of both g-C_3N_4 and Pb-doped g-C_3N_4 (Fig. 6b) samples. The Pb-doped g-C_3N_4 showed a noticeable increment of light absorption in the

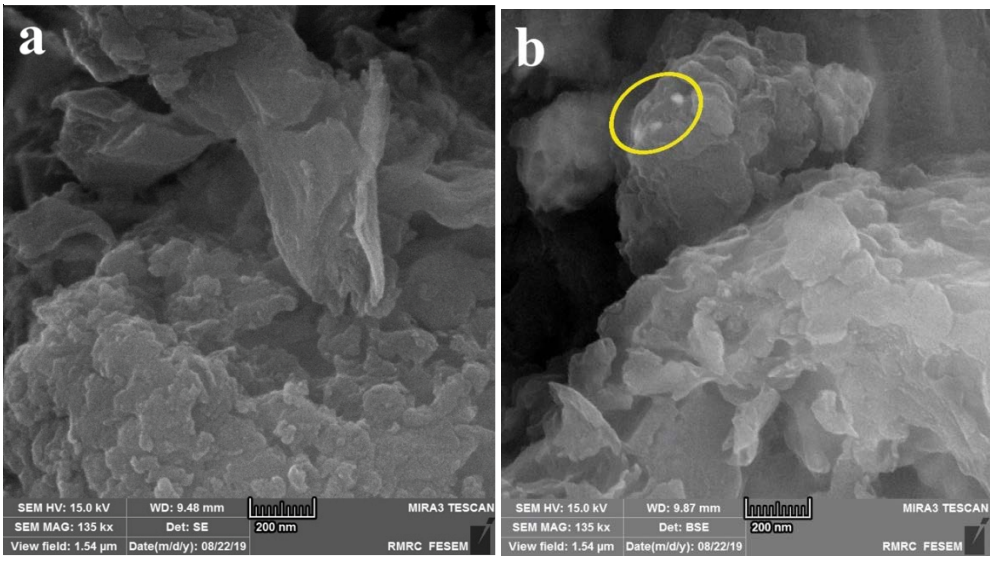

Fig. 3. FE-SEM analysis of both (a) g-C_3N_4 and (b) modified g-C_3N_4.

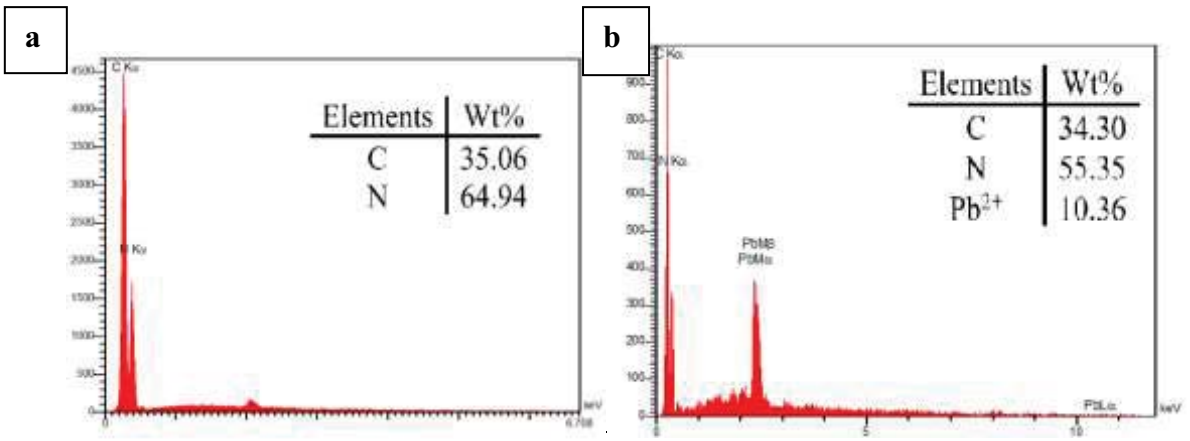

Fig. 4. EDX analysis of (a) g-C_3N_4 and (b) Pb-doped g-C_3N_4.

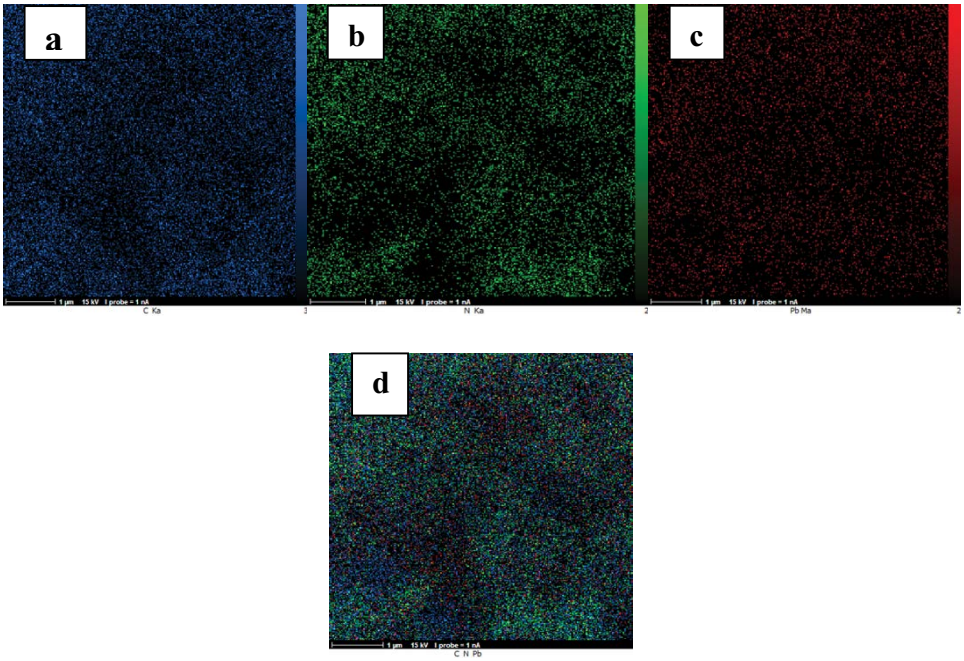

Fig. 5. EDX mapping analysis of Pb-doped g-C_3N_4 (a) C, (b) N, (c) Pb, (d) C, N, and Pb.

visible region compared to the g-C_3N_4. Moreover, a strong absorption at 320 nm was observed for g-C_3N_4, showing the ability g-C_3N_4 to absorb sunlight with an extensive wavelength [47]. The band gap was estimated from Fig. 6b using the Tauc formula as follows:

$$\alpha h\nu = \beta\left(h\nu - E_g\right)^r \quad (2)$$

where $h\nu$ is the incident photon energy, B is the Tauc parameter, and r equals 0.5, 0.66, 2, or 3 for the different electronic transition modes. The band gap of g-C_3N_4 was estimated to be 2.8 eV, close to the previously reported [48–50]. While it was estimated at 2.6 for Pb-doped g-C_3N_4. The Pb dopant incorporated in the g-C_3N_4 lattice acts as an intermediate band between the VB and CB of g-C_3N_4, leading to a slight reduction in band gap energy (increase in the visible light absorption of the Pb-doped g-C_3N_4). Also, the intensity of the visible peaks of the Pb-doped g-C_3N_4 is higher than that of the g-C_3N_4 due to the much lower band-gap of the Pb-doped g-C_3N_4 (2.6 eV) than the g-C_3N_4 (2.8 eV). The presence of lattice defects and the difference of crystal lattice parameters may be responsible for the decreased band gap [50].

3.1.6. BET analysis

Investigating the porosity, volume, and size distribution of particles, and the specific surface was performed based on N_2 adsorption and desorption at a constant temperature of liquid N_2 (77 K) via Micrometrics/ASAP2020 [51,52]. The nitrogen adsorption–desorption isotherms of g-C_3N_4 and Pb/g-C_3N_4 are represented in Fig. 7. Both samples present adsorption–desorption isotherms ascribed

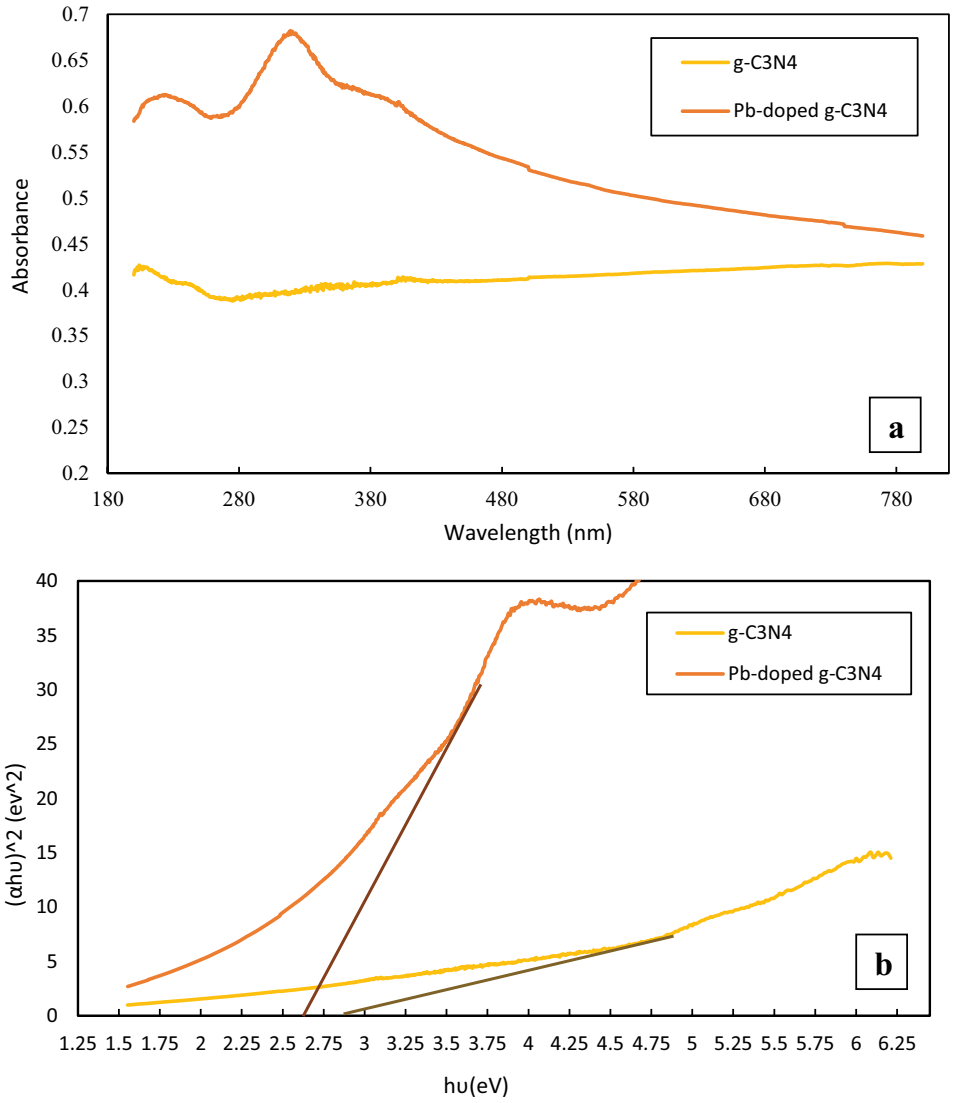

Fig. 6. (a) UV-Vis diffuse reflectance spectra and (b) Tauc plots of g-C_3N_4 and Pb-doped g-C_3N_4.

to type II with the mesoporous structure according to the IUPAC classification. The BET specific surface area of the Pb-doped g-C_3N_4 was estimated at 5.95 m^2/g, which is lower than that of the g-C_3N_4 (23.31 m^2/g) due to occupying pores by Pb. A similar trend was observed by Wang et al. [53]. They reported g-C_3N_4 has a greater surface area (19 m^2/g) than K-CN-10 (11 m^2/g) due to the enhanced interaction and degree of polymerization between the CN sheets after the incorporation of K to reduce the specific surface area [53]. In another study, Vignesh and Kang [54] observed lower surface areas for various concentrations (5%–40%) of Ag_2WO_4 doped on g-C_3N_4 than g-C_3N_4 [54].

3.2. Comparison of various synthesized composites

To compare the different synthesized composites (in regard to their Pb concentration), experiments were done under conditions that are pH = 5.5, time = 75 min, catalyst loading = 1.1 g/L, and cefixime initial concentration = 50 mg/L. As shown in Fig. 8, Pb/CN-2 sample shows the best performance compared to the others regard to photocatalytic degradational (after 60 min irradiation) and dark adsorption (after 75 min) values, which are 44% and 27%, respectively.

3.3. Study the effect of modified composite performance

In this study, the effect of four independent factors including the initial concentration of cefixime, initial pH, catalyst loading, and contact time on the removal efficiency was investigated using Design-Expert software (version 10.0.0) and i-Optimal method, which is a form of the response surface methodology (RSM) to attain the optimum conditions. Finally, 21 experiments were proposed by the Design-Expert.

To reach the maximum cefixime removal efficiency by obtaining the optimum conditions, the variables were performed as listed in Table 1.

Through various obtained optimum conditions, the conditions are shown in Fig. 9 with the desirability of 1.000

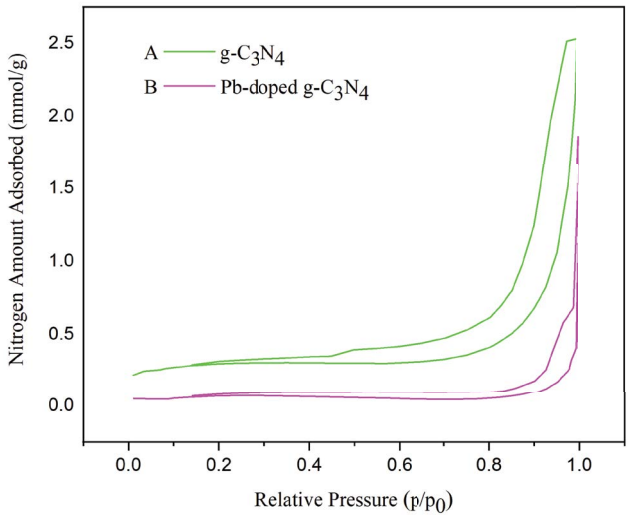

Fig. 7. Nitrogen adsorption–desorption isotherms of g-C_3N_4, and modified g-C_3N_4.

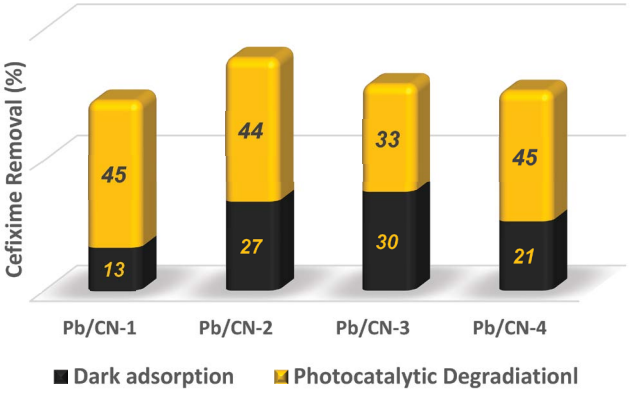

Fig. 8. Comparison of synthesized composites with various concentrations of Pb (1: Pb/CN-1, 2: Pb/CN-2, 3: Pb/CN-3, 4: Pb/CN-4).

Table 1
Experimental conditions set in Design-Expert

Variable	Range
Cefixime initial concentration, mg/L	10–70
Catalyst loading, g/L	0.5–2.1
Process time, min	60–160
pH	3–9
Cefixime removal efficiency, %	As much as possible

was chosen because of lower catalyst loading, pH neutral condition, and easier examination.

To investigate the effect of using modified g-C_3N_4 with Pb, its performance at the optimum conditions (pH = 6, catalyst loading = 1.7 g/L, and cefixime initial concentration = 46 mg/L) was compared, and as can be seen in Fig. 10, the results indicated that Pb-doped g-C_3N_4 has higher removal efficiency and photolytic activity than g-C_3N_4. The same results were reported by Gao et al. [39] due to adding Fe to g-C_3N_4 nanosheets.

3.4. Investigation the effect of various factors on cefixime removal

The following sections present the results for Pb-doped g-C_3N_4 under the effect of different factors.

3.4.1. Effect of the initial concentration of pollutant

Fig. 11 shows the cefixime removal vs. the initial concentration of cefixime in wastewater. At first, the cefixime removal efficiency increased by increasing the initial concentration of cefixime up to 30 mg/L due to the existence of many reaction active sites at low concentration, and there is not enough cefixime to make a noticeable collision between cefixime molecules and nanosheets. However, for concentrations above 30 mg/L, the amount of cefixime removal decreased significantly. This reduction in removal percentage can be related to the decreasing ratio of the active reaction sites on the catalyst's surface to the amount of cefixime molecules dissolved in water. Accordingly, the possibility of collision between cefixime molecules and nanosheets and removal percentage reduce [22,55].

3.4.2. Effect of catalyst loading

Pointed to the results from Design-Expert, the amount of catalyst loading has a significant effect on removal efficiency. By increasing the catalyst loading, photocatalyst's surface area with light and reaction active sites increased, and as shown in Fig. 12, cefixime removal efficiency increases [28,55].

3.4.3. Effect of irradiation time

Fig. 13 shows the effect of irradiation time on the removal percentage. In the first 120 min of irradiation, the removal efficiency increased continuously due to an increment in collision possibility between cefixime molecules and catalysts. After about 120 min of irradiation, the cefixime molecules which adsorb by nanoparticles but do not participate in the reaction, desorbed, and decrease the removal efficiency.

3.4.4. Effect of pH

The effect of solution pH on removal efficiency shown in Fig. 14. According to zeta potential results, nanosheets in pH range 3–9 have a negative charge and at pH = 3 catalyst's surface charge near to zero. At the strong acidic media, nanosheets have a lower negative charge, and therefore, cefixime molecules in cidic media are shaped to proton form. So, at low pH, attractive electrostatic forces of catalyst and protonated cefixime molecules are lower than high pH. As can be seen from Fig. 14, removal efficiency increases by increasing pH from 3 to 6.6. On the other hand, by increasing pH at the basic range, repulsive forces between nanosheets and electron pairs of amino and hydroxyl groups of cefixime molecules result in distance

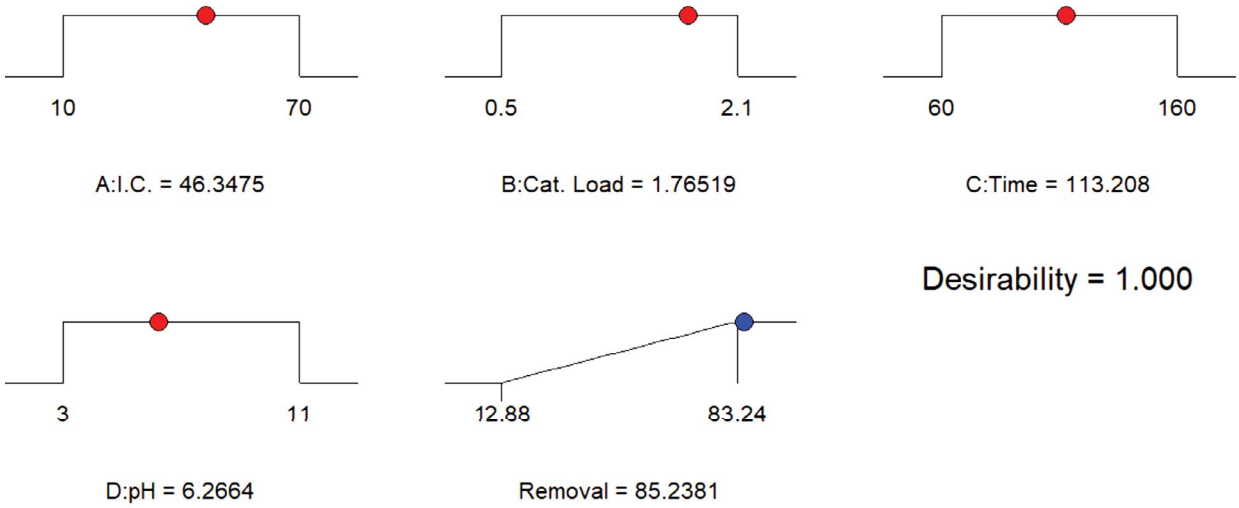

Fig. 9. Optimum conditions were chosen from Design-Expert.

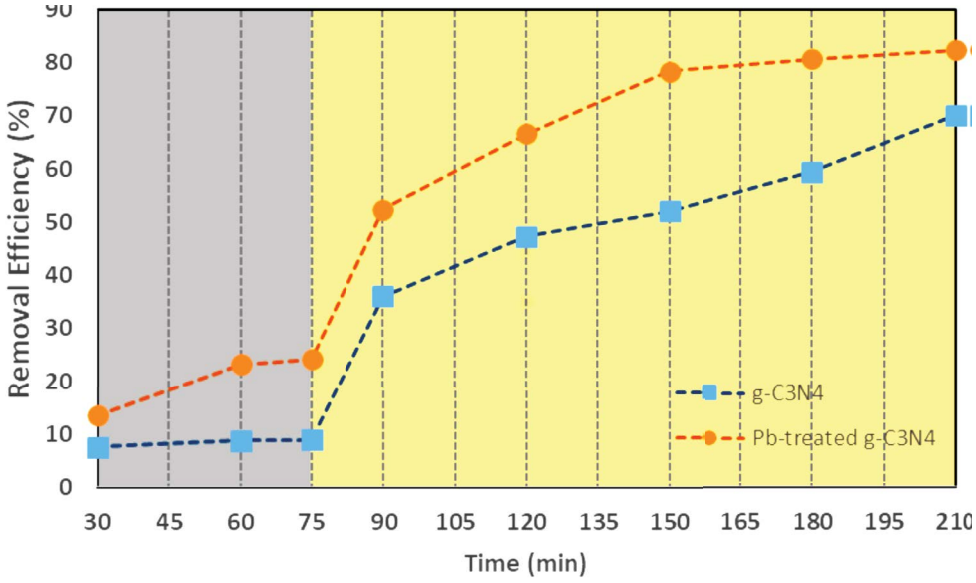

Fig. 10. Compare the g-C_3N_4 and Pb-doped g-C_3N_4 (cefixime initial concentration = 47 mg/L, catalyst loading = 1.7 g/L, and pH = 6.1).

cefixime molecules from the catalysts surface, and then removal efficiency reduces [56].

3.4.5. Performing experiments in continuous cycles

This section proposes an economic justification to remove cefixime from aqueous solutions by performing continuous cycles (Fig. 15). The experiments were performed at the optimum conditions mentioned before. After cefixime photodegradation in an aqueous solution under visible-light irradiation, the photocatalysts were centrifuged, washed three times with distilled water, and dried at 100°C for 4 h. Results showed removal efficiency decreases in more cycles which may be due to the presence of cefixime molecules or even intermediate substances on the photocatalyst's surface, which will compete for the active sites of the photocatalyst.

4. Conclusion

Graphitic carbon nitride and its modified form with Pb were synthesized with thermal polymerization method at 520°C for 2 h with 10°C/min heating rate. The prepared composites were used as active catalysts in visible light to remove cefixime from aqueous solutions. Pb-doped g-C_3N_4 modified the carbon nitride graphite using Pb^{2+} contained wastewater, which is an environmental pollutant, and was able to improve its performance to remove cefixime as a pharmaceutical pollutant. Various factors such as the initial concentration of the contaminant, catalyst loading, process time, and initial pH on cefixime removal were efficiently studied in this research, and Design-Expert software was used to design experiment conditions. The optimum conditions for removal efficiency with respect to the economic aspect and experiment's design are cefixime's initial

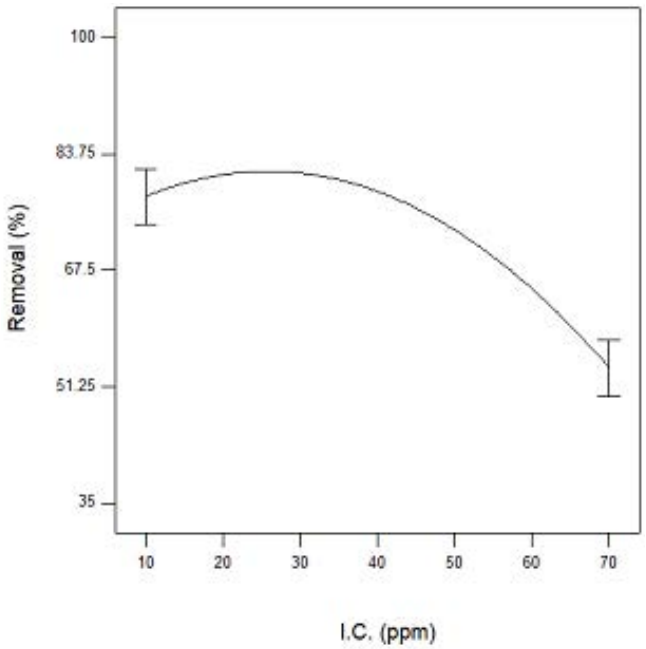

Fig. 11. Cefixime removal efficiency vs. initial concentration of cefixime for Pb-doped g-C_3N_4 (contact time = 125 min, catalyst loading = 0.9 g/L, and pH = 7).

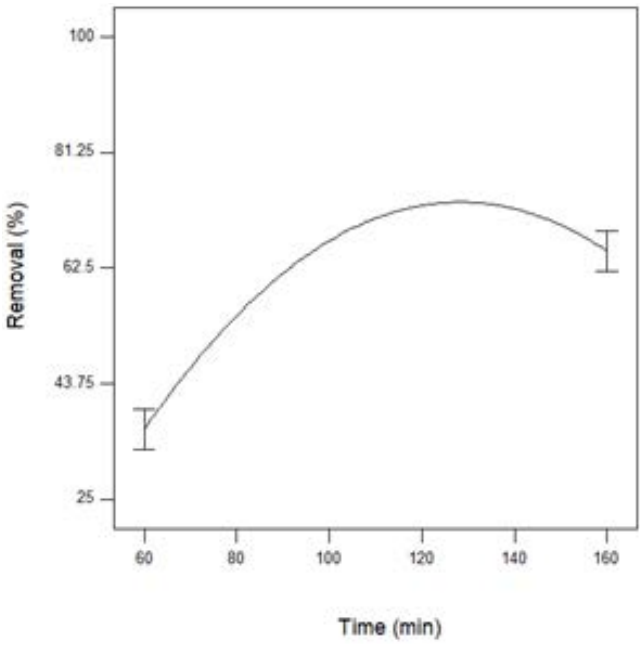

Fig. 13. Cefixime removal efficiency vs. contact time for Pb-doped g-C_3N_4 (cefixime initial concentration = 50 mg/L, catalyst loading = 0.9 g/L, and pH = 7).

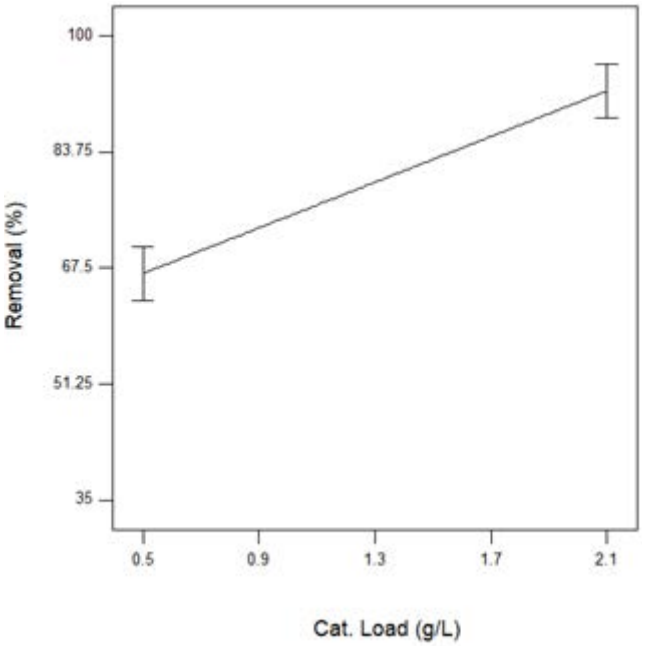

Fig. 12. Cefixime removal efficiency vs. catalyst loading for Pb-doped g-C_3N_4 (cefixime initial concentration = 50 mg/L, contact time = 125 min, and pH = 7).

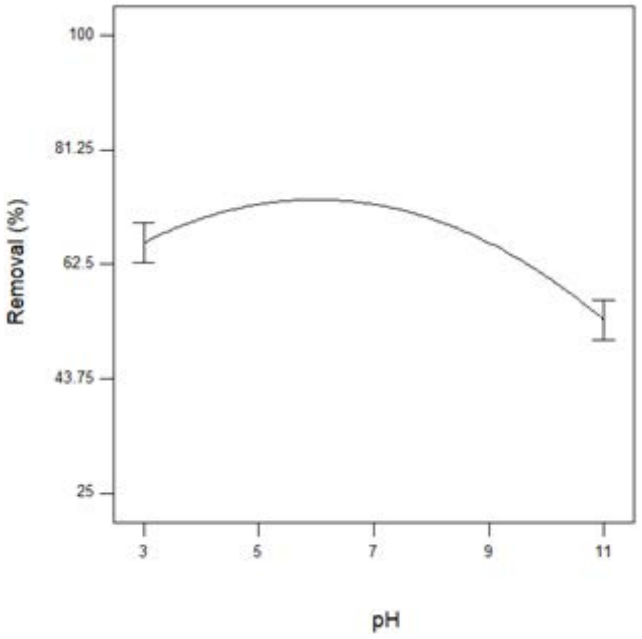

Fig. 14. Cefixime removal efficiency vs. initial pH for Pb-doped g-C_3N_4 (cefixime initial concentration = 50 mg/L, contact time = 125 min, and catalyst loading = 0.9 g/L).

concentration of 47 mg/L, 1.7 g/L catalyst loading, 113 min process time, and initial pH of 6.2. And also, the removal percentage at the mentioned conditions was 83.47%. The catalyst's performance in continuous cycles was investigated, and the results showed after 5 cycles, removal efficiency decreased to 37.06% from 83.47%. Moreover, the comparison between g-C_3N_4 and Pb-doped g-C_3N_4 showed better performance of novel catalyst than g-C_3N_4. The results of comparing the performance of Pb-doped g-C_3N_4 with previous work are given in Table 2.

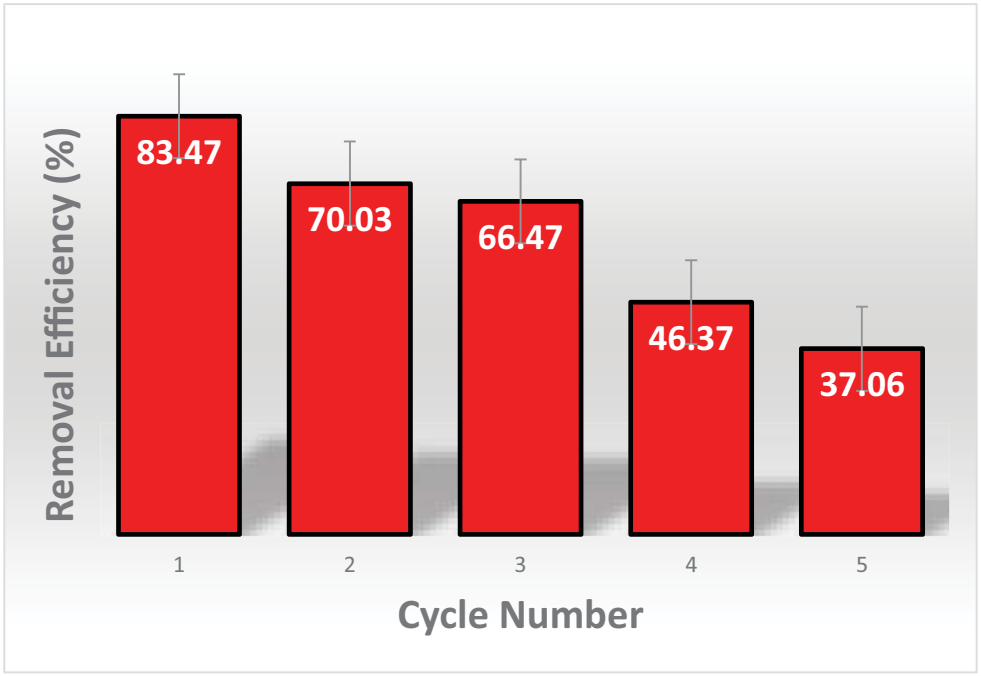

Fig. 15. Removal efficiency in continuous cycles (pH = 6, catalyst loading = 1.7 g/L, and cefixime initial concentration = 46 mg/L).

Table 2
Comparison of Pb-doped g-C_3N_4 performance with previous works

Adsorbent/Photocatalyst	Initial concentration (mg/L)	Adsorbent load (g/L)	Time (min)	pH	Removal (%)	Reference	Remarks
Nano-ZnO particles	40	–	50	6	81	[57]	Photocat.
NiO/nano-clinoptilolite	8	0.2	340	4.3	60	[56]	Photocat.
Cement	50	1.5 g	540	7	60	[30]	Ads.
TiO_2	5	0.001	60	–	90	[58]	Photocat.
n-TiO_2/graphene oxide/ titan grid sheets	5	6 cat. sheets	120	10	35	[28]	Photocatalytic ozonation
g-C_3N_4	50	1.7	115	6.2	67	This work	Photocat.
Pb-modified g-C_3N_4	50	1.7	115	6.2	84	This work	Photocat.

5. Perspective to future works

Specific research topics are recommended here to help future works:

- Investigate removing cefixime from real effluent using this composite;
- Use real Pb-containing effluent for modifying g-C_3N_4;
- Magnetizing the nanosheets for easier separation;
- Immobilizing the composite and use it in a fixed bed reactor;
- Investigation of the effect of temperature on the cefixime removal efficiency;
- Use this photocatalyst as a cost-effective efficient photocatalyst in industrial scale.

References

[1] R. Pawar, C.S. Lee, Heterogeneous Nanocomposite-Photocatalysis for Water Purification, William Andrew. Kidlington, Oxford, UK, 2015.
[2] M. Mezzelani, S. Gorbi, F. Regoli, Pharmaceuticals in the aquatic environments: evidence of emerged threat and future challenges for marine organisms, Mar. Environ. Res., 140 (2018) 41–60.
[3] C. Hignite, D.L. Azarnoff, Drugs and drug metabolites as environmental contaminants: chlorophenoxyisobutyrate and salicylic acid in sewage water effluent, Life Sci., 20 (1977) 337–341.
[4] A.W. Garrison, J.D. Pope, F.R. Allen, GC/MS Analysis of Organic Compounds in Domestic Wastewaters, L.H. Keith, Ed., Identification and Analysis of Organic Pollutants in Water, Ann Arbor Science Publishers, Ann Arbor, M.I., 1976, p. 517.
[5] H.M. Arshad, S. Gauhar, R. Bano, I.N. Muhammad, Development of HPLC–UV method for analysis of cefixime in raw materials and in capsule, Jordan J. Pharm. Sci., 2 (2009) 53–65.
[6] M. Iqbal, *Vicia faba* bioassay for environmental toxicity monitoring: a review, Chemosphere, 144 (2016) 785–802.
[7] M. Abbas, M. Adil, S. Ehtisham-ul-Haque, B. Munir, M. Yameen, A. Ghaffar, G.A. Shar, M.A. Tahir, M. Iqbal, *Vibrio fischeri* bioluminescence inhibition assay for ecotoxicity assessment: a review, Sci. Total Environ., 626 (2018) 1295–1309.

[8] M. Iqbal, M. Abbas, J. Nisar, A. Nazir, A. Qamar. Bioassays based on higher plants as excellent dosimeters for ecotoxicity monitoring: a review, Chem. Int., 5 (2019) 1–80.
[9] A. Jelić, M. Gros, M. Petrović, A. Ginebreda, D. Barceló, Chapter 1 – Occurrence and Elimination of Pharmaceuticals During Conventional Wastewater Treatment, H. Guasch, A. Ginebreda, A. Geiszinger, Eds., Emerging and Priority Pollutants in Rivers: Bringing Science into River Management Plans, Springer, Berlin, Heidelberg, 2012, pp. 1–23.
[10] M. Lindroos, D. Hörnström, G. Larsson, M. Gustavsson, A.J. van Maris, Continuous removal of the model pharmaceutical chloroquine from water using melanin-covered *Escherichia coli* in a membrane bioreactor, J. Hazard. Mater., 365 (2019) 74–80.
[11] R. Kallenborn, J. Fick, R. Lindberg, M. Moe, K.M. Nielsen, M. Tysklind, T. Vasskog, Pharmaceutical Residues in Northern European Environments: Consequences and Perspectives, K. Kümmerer, Ed., Pharmaceuticals in the Environment, Springer, Berlin, Heidelberg, 2008, pp. 61–74.
[12] A. Awwad, M. Amer, M. Al-Aqarbeh, TiO_2-kaolinite nanocomposite prepared from the Jordanian Kaolin clay: adsorption and thermodynamics of Pb(II) and Cd(II) ions in aqueous solution, Chem. Int., (2020).
[13] F. Minas, B.S. Chandravanshi, S. Leta, Chemical precipitation method for chromium removal and its recovery from tannery wastewater in Ethiopia, Chem. Int., 3 (2017) 291–305.
[14] K.B. Daij, S. Bellebia, Z. Bengharez, Comparative experimental study on the COD removal in aqueous solution of pesticides by the electrocoagulation process using monopolar iron electrodes, Chem. Int., 3 (2017) 420–427.
[15] K. Djehaf, A.Z. Bouyakoub, R. Ouhib, H. Benmansour, A. Bentouaf, A. Mahdad, N. Moulay, D. Bensaid, M. Ameri, Textile wastewater in Tlemcen (Western Algeria): impact, treatment by combined process, Chem. Int., 3 (2017) 314–318.
[16] Y.A. Neolaka, Y. Lawa, J.N. Naat, A.A. Riwu, M. Iqbal, H. Darmokoesoemo, H.S. Kusuma, The adsorption of Cr(VI) from water samples using graphene oxide-magnetic (GO-Fe_3O_4) synthesized from natural cellulose-based graphite (kusambi wood or *Schleichera oleosa*): study of kinetics, isotherms and thermodynamics, J. Mater. Res. Technol., 9 (2020) 6544–6556.
[17] M. Ahmad, I. Bhatti, K. Qureshi, N. Ahmad, J. Nisar, M. Zuber, A. Ashar, M. Khan, M. Iqbal, Graphene oxide supported $Fe_2(MoO_4)_3$ nanorods assembled round-ball fabrication via hydrothermal route and photocatalytic degradation of nonsteroidal anti-inflammatory drug, J. Mol. Liq., 301 (2020) 112343, doi: 10.1016/j.molliq.2019.112343.
[18] A.A. Adu, Y.A. Neolaka, A.A.P. Riwu, M. Iqbal, H. Darmokoesoemo, H.S. Kusuma, Synthesis, characterization and evaluation of swelling ratio on magnetic p53-poly (MAA-co-EGDMA)@GO-Fe_3O_4 (MIP@GO-Fe_3O_4)-based p53 protein and graphene oxide from kusambi wood (*Schleichera oleosa*), J. Mater. Res. Technol., 9 (2020) 11060–11068.
[19] K. Qureshi, M.Z. Ahmad, I.A. Bhatti, M. Zahid, J. Nisar, M. Iqbal, Graphene oxide decorated $ZnWO_4$ architecture synthesis, characterization and photocatalytic activity evaluation, J. Mol. Liq., 285 (2019) 778–789.
[20] S. Ata, I. Shaheen, S. Ghafoor, M. Sultan, F. Majid, I. Bibi, M. Iqbal, Graphene and silver decorated ZnO composite synthesis, characterization and photocatalytic activity evaluation, Diamond Relat. Mater., 90 (2018) 26–31.
[21] S. Ata, A. Rasool, A. Islam, I. Bibi, M. Rizwan, M.K. Azeem, M. Iqbal, Loading of cefixime to pH sensitive chitosan based hydrogel and investigation of controlled release kinetics, J. Biol. Macromol., 155 (2020) 1236–1244.
[22] X. Wang, K. Maeda, A. Thomas, K. Takanabe, G. Xin, J.M. Carlsson, K. Domen, M. Antonietti, A metal-free polymeric photocatalyst for hydrogen production from water under visible light, Nat. Mater., 8 (2009) 76–80.
[23] K.H. Leong, S.L. Liu, L.C. Sim, P. Saravanan, M. Jang, S. Ibrahim, Surface reconstruction of titania with g-C_3N_4 and Ag for promoting efficient electrons migration and enhanced visible light photocatalysis, Appl. Surf. Sci., 358 (2015) 370–376.
[24] D.H. Uresti, D.S. Martinez, L.T. Martinez, Novel visible light-driven $PbMoO_4$/g-C_3N_4 hybrid composite with enhanced photocatalytic performance, J. Photochem. Photobiol., A, 345 (2017) 21–26.
[25] Y. Hong, C. Li, G. Zhang, Y. Meng, B. Yin, Y. Zhao, W. Shi, Efficient and stable Nb_2O_5 modified g-C_3N_4 photocatalyst for removal of antibiotic pollutant, Chem. Eng. J., 299 (2016) 74–84.
[26] W. Wang, J. Fang, S. Shao, M. Lai, C. Lu, Compact and uniform TiO_2@g-C_3N_4 core-shell quantum heterojunction for photocatalytic degradation of tetracycline antibiotics, Appl. Catal., B, 217 (2017) 57–64.
[27] C. Li, S. Yu, H. Dong, C. Liu, H. Wu, H. Che, G. Chen, Z-scheme mesoporous photocatalyst constructed by modification of Sn_3O_4 nanoclusters on g-C_3N_4 nanosheets with improved photocatalytic performance and mechanism insight, Appl. Catal., B, 238 (2018) 284–293.
[28] M. Sheydaei, H.R.K. Shiadeh, B.A. Feiz, R. Ezzati, Preparation of nano n-TiO_2/graphene oxide/ titan grid sheets for visible light assisted photocatalytic ozonation of cefixime, Chem. Eng. J., 353 (2018) 138–146.
[29] S. Zavareh, T. Eghbalazar, Efficient and selective removal of cefixime form aqueous solution by a modified bionanocomposite, J. Environ. Chem. Eng., 5 (2017) 3337–3347.
[30] M.H. Rasoulifard, S. Khanmohammadi, A. Heidari, Adsorption of cefixime from aqueous solutions using modified hardened paste of Portland cement by perlite; optimization by Taguchi method, Water Sci. Technol., 74 (2016) 1069–1078.
[31] B. Zhu, P. Xia, W. Ho, J. Yu, Isoelectric point and adsorption activity of porous g-C_3N_4, Appl. Surf. Sci., 344 (2015) 188–195.
[32] K. Wang, Q. Li, B. Liu, B. Cheng, W. Ho, J. Yu, Sulfur-doped g-C_3N_4 with enhanced photocatalytic CO_2-reduction performance, Appl. Catal., B, 176 (2015) 44–52.
[33] Y. Ma, E. Liu, X. Hu, C. Tang, J. Wan, J. Li, J. Fan, A simple process to prepare few-layer g-C_3N_4 nanosheets with enhanced photocatalytic activities, Appl. Surf. Sci., 358 (2015) 246–251.
[34] Y. Tian, B. Chang, J. Lu, J. Fu, F. Xi, X. Dong, Hydrothermal synthesis of graphitic carbon nitride–Bi_2WO_6 heterojunctions with enhanced visible light photocatalytic activities, ACS Appl. Mater. Interfaces, 5 (2013) 7079–7085.
[35] I.F. Teixeira, E.C. Barbosa, S.C.E. Tsang, P.H. Camargo, Carbon nitrides and metal nanoparticles: from controlled synthesis to design principles for improved photocatalysis, Chem. Soc. Rev., 47 (2018) 7783–7817.
[36] H. Zhao, Y. Dong, P. Jiang, H. Miao, G. Wang, J. Zhang, In situ light-assisted preparation of MoS_2 on graphitic C_3N_4 nanosheets for enhanced photocatalytic H_2 production from water, J. Mater. Chem., A, 3 (2015) 7375–7381.
[37] P. Niu, L. Zhang, G. Liu, H.M. Cheng, Graphene-like carbon nitride nanosheets for improved photocatalytic activities, Adv. Funct. Mater., 22 (2012) 4763–4770.
[38] S. Tonda, S. Kumar, S. Kandula, V. Shanker, Fe-doped and-mediated graphitic carbon nitride nanosheets for enhanced photocatalytic performance under natural sunlight, J. Mater. Chem. A, 2 (2014) 6772–6780.
[39] J. Gao, Y. Wang, S. Zhou, W. Lin, Y. Kong, A facile one-step synthesis of Fe-doped g-C_3N_4 nanosheets and their improved visible-light photocatalytic performance, ChemCatChem, 9 (2017) 1708–1715.
[40] X. Wang, X. Chen, A. Thomas, X. Fu, M. Antonietti, Metal-containing carbon nitride compounds: a new functional organic–metal hybrid material, Adv. Mater., 21 (2009) 1609–1612.
[41] J. Gao, J. Wang, X. Qian, Y. Dong, H. Xu, R. Song, C. Yan, H. Zhu, Q. Zhong, G. Qian, One-pot synthesis of copper-doped graphitic carbon nitride nanosheet by heating Cu–melamine supramolecular network and its enhanced visible-light-driven photocatalysis, J. Solid State Chem., 228 (2015) 60–64.
[42] J. Tian, Q. Liu, A.M. Asiri, A.H. Qusti, A.O.A. Youbi, X. Sun, Ultrathin graphitic carbon nitride nanosheets: a novel peroxidase mimetic, Fe doping–mediated catalytic performance enhancement and application to rapid, highly sensitive optical detection of glucose, Nanoscale, 5 (2013) 11604–11609.
[43] X. She, J. Wu, J. Zhong, H. Xu, Y. Yang, R. Vajtai, J. Lou, Y. Liu, D. Du, H. Li, Oxygenated monolayer carbon nitride for excellent

photocatalytic hydrogen evolution and external quantum efficiency, Nano Energy, 27 (2016) 138–146.
[44] Y. Zhong, Z. Wang, J. Feng, S. Yan, H. Zhang, Z. Li, Z. Zou, Improvement in photocatalytic H_2 evolution over g-C_3N_4 prepared from protonated melamine, Appl. Surf. Sci., 295 (2014) 253–259.
[45] J. Xu, H.T. Wu, X. Wang, B. Xue, Y.X. Li, Y. Cao, A new and environmentally benign precursor for the synthesis of mesoporous g-C_3N_4 with tunable surface area, Phys. Chem. Chem. Phys., 15 (2013) 4510–4517.
[46] F. Dong, Z. Wang, Y. Sun, W.K. Ho, H. Zhang, Engineering the nanoarchitecture and texture of polymeric carbon nitride semiconductor for enhanced visible light photocatalytic activity, J. Colloid Interface Sci., 401 (2013) 70–79.
[47] G. Zhang, T. Zhang, B. Li, S. Jiang, X. Zhang, L. Hai, X. Chen, W. Wu, An ingenious strategy of preparing TiO_2/g-C_3N_4 heterojunction photocatalyst: in situ growth of TiO_2 nanocrystals on g-C_3N_4 nanosheets via impregnation-calcination method, Appl. Surf. Sci., 433 (2018) 963–974.
[48] L.Y. Chen, W.D. Zhang, In_2O_3/g-C_3N_4 composite photocatalysts with enhanced visible light driven activity, Appl. Surf. Sci., 301 (2014) 428–435.
[49] D. Jiang, L. Chen, J. Xie, M. Chen, Ag_2S/g-C_3N_4 composite photocatalysts for efficient Pt-free hydrogen production. The co-catalyst function of Ag/Ag_2S formed by simultaneous photodeposition, Dalton Trans., 43 (2014) 4878–4885.
[50] J. Lang, M. Liu, Y. Su, L. Yan, X. Wang, Fabrication of the heterostructured $CsTaWO_6$/Au/g-C_3N_4 hybrid photocatalyst with enhanced performance of photocatalytic hydrogen production from water, Appl. Surf. Sci., 358 (2015) 252–260.
[51] H. Wang, X. Yuan, Y. Wu, G. Zeng, X. Chen, L. Leng, H. Li, Synthesis and applications of novel graphitic carbon nitride/metal-organic frameworks mesoporous photocatalyst for dyes removal, Appl. Catal., B, 174 (2015) 445–454.
[52] K.S. Sing, Reporting physisorption data for gas/solid systems with special reference to the determination of surface area and porosity (Recommendations 1984), Pure Appl. Chem., 57 (1985) 603–619.
[53] Y. Wang, S. Zhao, Y. Zhang, J. Fang, Y. Zhou, S. Yuan, C. Zhang, W. Chen, One-pot synthesis of K-doped g-C_3N_4 nanosheets with enhanced photocatalytic hydrogen production under visible-light irradiation, Appl. Surf. Sci., 440 (2018) 258–265.
[54] K. Vignesh, M. Kang, Facile synthesis, characterization and recyclable photocatalytic activity of Ag_2WO_4@g-C_3N_4, Mater. Sci. Eng., B, 199 (2015) 30–36.
[55] C. Shaniba, M. Akbar, K. Ramseena, P. Raveendran, B.N. Narayanan, R.M. Ramakrishnan, Sunlight-assisted oxidative degradation of cefixime antibiotic from aqueous medium using TiO_2/nitrogen doped holey graphene nanocomposite as a high performance photocatalyst, J. Environ. Chem. Eng., 8 (2020) 102204, doi: 10.1016/j.jece.2018.02.012.
[56] A. Pourtaheri, A.N. Ejhieh, Photocatalytic properties of incorporated NiO onto clinoptilolite nano-particles in the photodegradation process of aqueous solution of cefixime pharmaceutical capsule, Chem. Eng. Res. Des., 104 (2015) 835–843.
[57] M. Visalakshi, G.S. Bai, V. Sinduri, G. Praveena, G. Ushasree, G. Swapna, Photocatalytic degradation of outdated antibiotics by nano-crystalline ZnO, International Conference on Advanced Nanomaterials & Emerging Engineering Technologies, IEEE, Chennai, India, 2013, pp. 409–411.
[58] S. Sahraeian, V. Alipour, O. Rahmanian, High efficient degradation of cefixime using UV/TiO_2 photocatalytic process: a comparison between photocatalytic and photolytic, Hormozgan Med. J., 21 (2017) 159–168.